

# Mega-Hertz Gravitational Waves from Neutron Star Mergers

---

**Jorge Casalderrey-Solana,<sup>a</sup> David Mateos,<sup>b,a</sup> Mikel Sanchez-Garitaonandia<sup>a,c</sup>**

<sup>a</sup>*Departament de Física Quàntica i Astrofísica and Institut de Ciències del Cosmos (ICC), Universitat de Barcelona, Martí i Franquès 1, ES-08028, Barcelona, Spain.*

<sup>b</sup>*Institució Catalana de Recerca i Estudis Avançats (ICREA), Passeig Lluís Companys 23, ES-08010, Barcelona, Spain.*

<sup>c</sup>*CPHT, CNRS, École Polytechnique, IP Paris, F-91128 Palaiseau, France*

**ABSTRACT:** Neutron star mergers provide a unique laboratory for the study of strong-field gravity coupled to Quantum Chromodynamics in extreme conditions. The frequencies and amplitudes of the resulting gravitational waves encode invaluable information about the merger. Simulations to date have shown that these frequencies lie in the kilo-Hertz range. They have also shown that, if Quantum Chromodynamics possesses a first-order phase transition at high baryon density, then this is likely to be accessed during the merger dynamics. Here we show that this would result in the nucleation of superheated and/or supercompressed bubbles whose subsequent dynamics would produce gravitational waves in the Mega-Hertz range. We estimate the amplitude of this signal and show that it may fall within the expected sensitivity of future superconducting radio-frequency cavity detectors for mergers at distances up to tens of Mega-parsecs.

---

## Contents

<b>1</b>	<b>Introduction</b>	<b>1</b>
<b>2</b>	<b>Frequency</b>	<b>3</b>
<b>3</b>	<b>Characteristic strain</b>	<b>8</b>
<b>4</b>	<b>Discussion</b>	<b>10</b>

---

## 1 Introduction

The revolutionary discovery of gravitational waves (GW) has opened two unprecedented windows into the Universe: one into the strong-field regime of gravity, and another one into the dynamics of quantum matter. These two aspects are often intertwined. This is beautifully illustrated by neutron star (NS) mergers, in which quarks and gluons described by Quantum Chromodynamics (QCD) interact in the strong gravitational field sourced by the quarks and gluons themselves.

Most of the merger dynamics can be accurately described by numerical simulations of magneto-hydrodynamics coupled to general relativity (for a review, see e.g. [1]). One robust conclusion of these simulations is that the characteristic lifetime of the system is of order of several, possibly 10, milliseconds (ms). These simulations take as an input the properties of QCD, in particular its Equation of State (EoS). At zero baryon density the EoS can be reliably determined via the lattice formulation of QCD. In contrast, the famous sign problem [2] renders this tool inapplicable at the baryon densities of interest for NS physics. In particular, it is unknown whether QCD possesses first-order phase transitions (FOPT) in this region. Nevertheless, a variety of arguments suggest that at least two FOPT may be present [3–6], as sketched in Fig. 1. One is the transition from hadronic matter to deconfined, quark matter. The other is the transition from a non-superconducting to a color-superconducting phase. We emphasize that, while these transitions are well motivated, at the theoretical level their existence cannot be rigorously established at present. NS mergers have the potential to establish this experimentally, possibly in combination with heavy ion collision experiments. To realise this potential, a theoretical understanding of the imprints of a phase transition on the GW spectrum is indispensable.

Numerical simulations of NS mergers based on EoS with a hadronic-quark matter phase transition include [7–12]. These studies have shown that the dynamics of the merger results in the formation of regions in which the matter is sufficiently heated and/or compressed so that the thermodynamically preferred phase is the quark-matter phase. We will generically

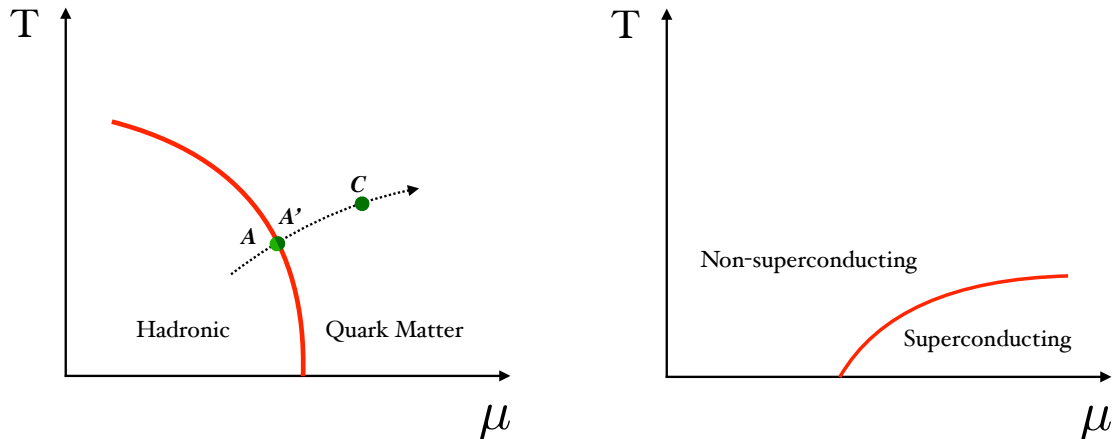


**Figure 1.** Two possible phase transitions in QCD, indicated by the solid red curves.  $T$  and  $\mu$  are the temperature and the baryon chemical potential, respectively. The dotted black curve on the left panel shows a possible evolution of a region of a NS merger as this region is heated and/or compressed. The points dubbed  $A$ ,  $A'$  and  $C$  correspond to the states shown in Fig. 3.

refer to these regions as “Hot or Compressed Spots”, or HoCS for short — see Fig. 2. The characteristic size of these HoCS is [12]

$$L \simeq 5 \text{ km}. \quad (1.1)$$

To our knowledge, no simulation based on an EoS that includes a transition to a color-superconducting phase has been performed. Nevertheless, existing simulations have shown that the merger leads to the formation of cold quark-matter regions in which the baryon density can be ten times larger than the nuclear saturation density. This makes it conceivable that color-superconducting matter may be formed in NS mergers.

Numerical simulations have shown that the *presence* of HoCS affects the overall merger dynamics, mainly because of a softening of the EoS, and leads to detectable modifications of the GW spectrum in the usual kilo-Hertz (kHz) frequency range. One may think of this as a “macroscopic” consequence of the phase transition. However, to the best of our knowledge, the *phase transition dynamics* in HoCS has not been previously considered. The purpose of this paper is to show that this dynamics leads to a characteristic signal in the Mega-Hertz (MHz) range. One may think of this as a “microscopic” consequence of the phase transition. We will see that this conclusion is extremely robust since it only depends on generic properties of a FOPT. Therefore we do not need to commit ourselves to a particular type of FOPT. The only assumptions we need to make are that some FOPT is present in QCD and that this is accessed by the merger dynamics.

The key idea is that the millisecond characteristic time scale for the evolution of the merger is much longer than the characteristic nuclear time scale,  $1 \text{ fm} \simeq 10^{-23} \text{ s}$ . This huge separation of scales means that, from the viewpoint of QCD processes, the merger evolution is adiabatic to an extremely good approximation. In turn, this implies that the HoCS are initially born as carefully prepared metastable regions of superheated and/or

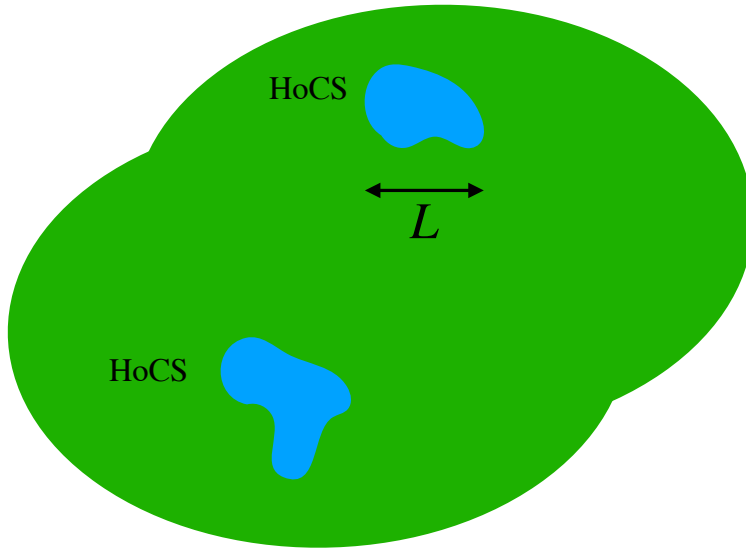


**Figure 2.** Formation of HoCS in the merger of two NS. The picture corresponds to a snapshot at a time before bubble nucleation begins. This means that the green region is in a state in the lower stable branch in Fig. 3, whereas the HoCS are in a state in the lower metastable branch between points  $A$  and  $B$ . Nucleation and the subsequent dynamics are shown in Fig. 4.

supercompressed matter. Once the superheating or supercompression are large enough, namely once the HoCS is sufficiently deep into the metastable branch, bubbles of the stable phase begin to nucleate. The point where this happens is labeled “ $B$ ” in Fig. 3. These bubbles then expand to a macroscopic size and collide, leaving behind long-lived sound waves propagating on top of the stable phase, as illustrated in Fig. 4. As we will explain below, this dynamics gives rise to a characteristic GW spectrum whose peak frequency is in the MHz range.

As usual, we work with units such that  $\hbar = c = 1$ .

## 2 Frequency

We begin by noting that the dynamics of a FOPT in a NS merger is very similar to that of a cosmological FOPT (for a review, see e.g. [13]), except for the fact that in the cosmological case the metastable phase is supercooled. In this case there is a compelling physical picture that emerges from the large body of work developed over several decades. Here we will take advantage of this picture to give an order-of-magnitude estimate of the GW signal in a NS merger. A more refined analysis will be presented elsewhere [14].

In the cosmological case the separation of scales is provided by the fact that the expansion rate of the Universe,  $H^{-1}$ , with  $H$  the Hubble rate, is much longer than the microscopic time scale given by the inverse of the local temperature,  $T^{-1}$ . As the Universe expands and cools down it eventually enters the metastable phase. At some point bubbles of the stable phase begin to nucleate. These bubbles then grow and collide and eventually

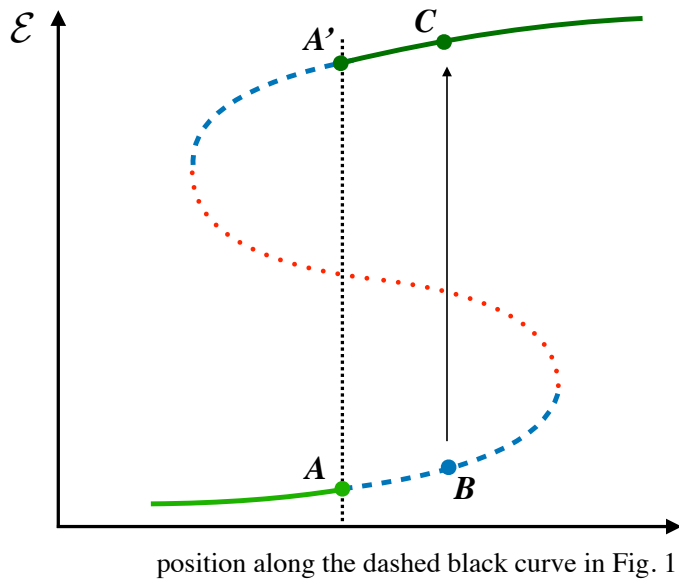


**Figure 3.** Energy density as a function of the position along the dashed black curve in Fig. 1. Both  $T$  and  $\mu$  increase from left to right. The dotted black vertical line indicates the location of the phase transition, determined by the condition that the states  $A$  and  $A'$  have the same free energy density. The solid green curves indicate stable states. States on the dashed blue curves are metastable. The dotted red curve corresponds to unstable states. As a region is heated or compressed it enters the lower metastable branch. At the point  $B$  the condition (2.11) is satisfied. At this point bubbles of the preferred state  $C$  on the upper stable branch are quickly nucleated.

leave behind a superposition of long-lived sound waves propagating on the stable phase. At sufficiently late times turbulence may also develop. Although each of these processes contributes to the GW spectrum, for many models of the transition it has been shown that the dominant contribution comes from collisions of sound waves with one another [15]. As a first approximation, we will assume that the same may be true in a NS merger. We will now determine the peak frequency of the GWs, and in the next section we will estimate their characteristic strain.

Let  $R$  be the mean bubble centre separation at the end of the phase transition, as illustrated in Fig. 4. This scale is inherited by the sound waves that are left behind after the bubbles collide, and it is further imprinted on the GWs produced by the subsequent fluid dynamics. The peak GW frequency,  $\lambda$ , is therefore [13, 16]

$$\lambda \simeq R. \quad (2.1)$$

Nucleated bubbles grow with a constant bubble wall velocity  $v_w$ . A reasonable ballpark value for this quantity is

$$v_w \simeq 0.1. \quad (2.2)$$

We will see below that, if  $\beta^{-1}$  denotes the duration of the phase transition, then the mean

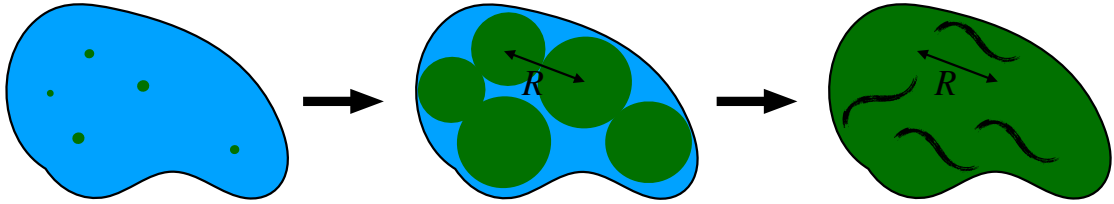


**Figure 4.** Phase transition dynamics inside a HoCS. First, microscopic bubbles of the stable phase are nucleated inside the metastable phase (left). The bubbles then grow to a macroscopic size  $R$  and collide (center), eventually leaving behind long-lived sound waves of characteristic size  $R$  propagating on top of the stable phase (right). Once some region of the NS enters the metastable region, as in Fig. 2, it takes a time of order  $\tau \simeq 1$  ms for bubbles to begin to nucleate, as depicted in the left panel of this figure. It then takes a time  $\beta^{-1} \simeq 6 \mu\text{s}$  to go from the left panel to the right panel. Finally, the lifetime of the sound waves in the right panel is again of order  $\tau \simeq 1$  ms.

bubble centre separation is given by

$$R = (8\pi)^{1/3} \frac{v_w}{\beta}. \quad (2.3)$$

Consequently, in order to determine the GW wavelength, we must estimate the duration of the phase transition. For this purpose we need to recall how the phase transition takes place dynamically.

Suppose that some region of the NS follows the trajectory indicated by the dashed black curve in Fig. 1(left). The energy density of the available phases of the system as  $T$  and  $\mu$  vary along this curve is shown in Fig. 3. The multivaluedness of this plot is a hallmark of a FOPT. The difference in the energy density between points  $A'$  and  $A$  corresponds to the latent heat. A similar multivaluedness and a similar discontinuity across the phase transition are found in the entropy density and the baryon density, which also increase as the phase transition is crossed along the trajectory in Fig. 1(left). The free energy density is multivalued but continuous across the phase transition. The location of the phase transition, indicated by the dotted black vertical line, is determined by the condition that the free energy densities of points  $A$  and  $A'$  are equal to one another. The different colors in Fig. 3 indicate stable, metastable and unstable states. Note that only the stable states are shown in the phase diagram of Fig. 1(left), whose hadronic and quark-matter phases correspond to the lower and upper stable branches of Fig. 3, respectively. Points  $A$  and  $A'$  are approached as the phase transition curve is approached along the hadronic and the quark-matter phases, respectively. Although the quantitative details of Fig. 3 depend on the specific trajectory in Fig. 1(left), its qualitative features only depend on the fact that this trajectory crosses a line of FOPTs.

The reason why metastable (and unstable) states are not represented in Fig. 1 is that, by definition, the phase diagram only captures the *static* properties of the system, namely the globally thermodynamically stable states. Yet, metastable states play a crucial role in the way the FOPT takes place *dynamically*. Indeed, as the region in the NS is heated and/or compressed along the trajectory of Fig. 1(left), the corresponding state moves along

the lower stable branch in Fig. 3 until it eventually enters the lower metastable branch. Once this happens, bubbles of the stable phase can begin to nucleate. On general grounds, the probability per unit volume and per unit time for this to happen takes the form

$$\frac{dP}{dt d^3x} = \Lambda^4 e^{-S[\Lambda]}. \quad (2.4)$$

In this equation,  $\Lambda$  is a linear combination of the temperature and the chemical potential that depends on the specific point on the metastable branch. In a NS merger the natural value for this scale is (see e.g. [17])

$$\Lambda^4 \simeq 1 \text{ GeV}/\text{fm}^3. \quad (2.5)$$

$S$  is the action of the critical bubble at the same point in the metastable phase. The critical bubble is the bubble for which the inward-pointing force due to the surface tension is exactly balanced by the outward-pointing force due to the pressure difference between the inside and the outside of the bubble. The action of this bubble controls the bubble nucleation probability in the semiclassical approximation, hence the exponential dependence in (2.4). The value of  $S$  is infinite at the point  $A$  where the metastable phase meets the stable phase, and it decreases until it reaches zero at the turning point where the metastable phase meets the unstable phase. At an arbitrary point on the metastable branch the value of  $S$  depends on the corresponding values of the temperature and the chemical potential.

Let  $t_c$  be the time when the system enters the metastable phase. At a later time  $t > t_c$ , the fraction of the HoCS volume still in the metastable phase is [18, 19]

$$q(t) = e^{-I(t)}, \quad (2.6)$$

with

$$I(t) = \int_{t_c}^t dt' \frac{4}{3} \pi v_w^3 (t - t')^3 \Lambda^4 e^{-S(t')}. \quad (2.7)$$

Eqn. (2.6) is easily interpreted. The integrand is the volume of a bubble nucleated at a time  $t_c < t' < t$  multiplied by the bubble nucleation probability at that time. At early times  $I(t) \ll 1$  and

$$q(t) \simeq 1 - I(t). \quad (2.8)$$

This is the expected expression if bubble overlaps are ignored. The exponentiation in (2.6) accounts for these overlaps.

Since the integrand in (2.7) is dominated by times  $t'$  near  $t$ , we can Taylor-expand the action to linear order in  $t - t'$  to obtain

$$q(t) \simeq \exp \left[ -\frac{4}{3} \pi v_w^3 \Lambda^4 e^{-S(t)} 6\beta^{-4} \right], \quad (2.9)$$

where

$$\beta = -\frac{dS}{dt}. \quad (2.10)$$

The phase transition takes place at the time  $t_f$  where the exponent in (2.9) becomes unity, namely when

$$8\pi v_w^3 \Lambda^4 e^{-S(t_f)} \beta^{-4} = 1. \quad (2.11)$$

At this time a fraction  $1/e \simeq 37\%$  of the volume remains in the metastable phase. Expanding (2.9) around  $t_f$  we see that  $q(t)$  takes the very simple form

$$q(t) \simeq \exp \left[ -e^{\beta(t-t_f)} \right]. \quad (2.12)$$

This equation justifies the interpretation of  $\beta^{-1}$  (evaluated at  $t = t_f$ ) as the duration time of the transition. This time can be determined from the condition (2.11). To do so, we first use the chain rule to rewrite (2.10) as

$$\beta\tau = -\Lambda \frac{dS}{d\Lambda}, \quad (2.13)$$

where

$$\frac{1}{\tau} = \frac{1}{\Lambda} \frac{d\Lambda}{dt}. \quad (2.14)$$

The time  $\tau$  is the characteristic evolution time of the system which, based on NS merger simulations, is of order

$$\tau \simeq 1 \text{ ms}. \quad (2.15)$$

Generically, we expect the dimensionless derivative of  $S$  on the right-hand side of (2.13) to be of the same order as  $S$  itself. Therefore

$$\beta\tau \simeq S, \quad (2.16)$$

where  $S$  is understood to be evaluated at  $t = t_f$ . Substituting in (2.11) we then have

$$S^4 e^S \simeq 8 v_w^3 \tau^4 \Lambda^4 \simeq 10^{81}, \quad (2.17)$$

where we have used (2.2), (2.5) and (2.15). The number on the right-hand side comes from the huge hierarchy between the microscopic scale,  $\Lambda$ , and the macroscopic scale,  $\tau$ . This hierarchy is responsible for the adiabaticity of the evolution until bubbles begin to nucleate. Solving for the action we find

$$S \simeq 166, \quad (2.18)$$

and using (2.15) and (2.16) we determine the duration of the phase transition to be

$$\beta^{-1} \simeq \frac{1}{166} \text{ ms} \simeq 6 \mu\text{s}. \quad (2.19)$$

We can now determine the mean bubble center separation. The number of bubbles per unit volume at a time  $t > t_c$  is the integral until that time of the probability of nucleating bubbles in the metastable phase, times the available volume of metastable phase. Thus at a time  $t > t_c$  this is given by

$$n_{\text{bubble}}(t) = \int_{t_c}^t dt' q(t') \frac{dP}{dt' d^3x}. \quad (2.20)$$



Using the Taylor expansions around  $t_f$  introduced above, this becomes

$$\begin{aligned}
n_{bubble}(t) &= \Lambda^4 e^{-S(t_f)} \int_{t_c}^t dt' \exp \left[ -e^{\beta(t-t_f)} \right] e^{\beta(t-t_f)} \\
&= -\Lambda^4 e^{-S(t_f)} \beta^{-1} \int_{t_c}^t dt' \frac{d}{dt'} \exp \left[ -e^{\beta(t-t_f)} \right] \\
&= \Lambda^4 e^{-S(t_f)} \beta^{-1} \left[ 1 - q(t) \right].
\end{aligned} \tag{2.21}$$

At late times  $q(t \rightarrow \infty) \rightarrow 0$  and, using (2.11), we arrive at the final density of bubbles

$$n_{bubble} = \frac{\beta^3}{8\pi v_w^3}. \tag{2.22}$$

Since the mean bubble center separation is defined as  $R = (n_{bubble})^{-1/3}$ , this leads to (2.3). Using (2.1), (2.2) and (2.19) we finally arrive at the value

$$\lambda \simeq R \simeq 530 \text{ m} \tag{2.23}$$

for the GW wavelength, corresponding to a frequency

$$f \simeq 0.6 \text{ MHz}. \tag{2.24}$$

To recap, once some region of the NS enters the metastable region, as in Fig. 2, it takes a time of order  $\tau \simeq 1$  ms for bubbles to begin to nucleate, as depicted in the left panel of Fig. 4. The typical number of nucleated bubbles in one of these regions is of order

$$N_{bubble} = n_{bubble} \times L^3 = \frac{L^3}{R^3} \simeq 840. \tag{2.25}$$

Once bubble nucleation starts, it takes a time of order  $\beta^{-1} \simeq 6 \mu\text{s}$  for the phase transition to complete, namely to go from the left panel to the right panel of Fig. 4. Finally, the lifetime of the sound waves left behind after the transition, as illustrated in the right panel of Fig. 4, is again of order  $\tau \simeq 1$  ms. The dominant contribution to GW emission comes from these sound waves, and these GWs have frequency  $f \simeq 0.6$  MHz.

### 3 Characteristic strain

As explained above, we follow the physical picture developed in the cosmological case and assume that the dominant GW production mechanism is due to the long-lived sound waves left behind after all the bubbles have collided. In the cosmological case, the GW energy density produced by sound waves can be estimated as

$$\rho_{\text{GW}} \simeq (8\pi G) v_f^4 (\mathcal{E} + \mathcal{P})^2 \Delta t R \bar{\Omega}_{\text{GW}}. \tag{3.1}$$

A detailed derivation of this formula can be found in e.g. [16]. We will not reproduce the derivation here, but we will provide intuition for the origin of each term.

$G$  is Newton's constant, related to the reduced Planck mass through

$$(8\pi G)^{-1/2} = M_p \simeq 2.4 \times 10^{18} \text{ GeV}. \quad (3.2)$$

The factor of  $G$  in (3.1) encodes the fact that there are no GWs if gravity is turned off.

$\mathcal{E}$ ,  $\mathcal{P}$  and  $v_f^2$  are the energy density, the pressure and the root mean velocity of the fluid in the HoCS left behind by the bubble collisions, as illustrated in Fig. 4(right). We take  $\mathcal{E}$  and  $\mathcal{P}$  to be of order (see e.g. [17])

$$\mathcal{E} \simeq \mathcal{P} \simeq 1 \text{ GeV}/\text{fm}^3. \quad (3.3)$$

GWs are metric perturbations,  $h_{ij}(t, \mathbf{x})$ , sourced by the transverse-traceless part of the energy-momentum tensor,  $T_{ij}^{TT}(t, \mathbf{x})$ . For sound waves on a fluid we have

$$T_{ij}^{TT} \sim (\mathcal{E} + \mathcal{P})v_iv_j. \quad (3.4)$$

The energy density in GWs scales as

$$\rho_{\text{GW}} \propto \dot{h}_{ij}(t, \mathbf{x})\dot{h}^{ij}(t, \mathbf{x}). \quad (3.5)$$

This leads to the  $v_f^4(\mathcal{E} + \mathcal{P})^2$  factor in (3.1).

$\Delta t$  is the effective time duration of the source for the purpose of determining  $\rho_{\text{GW}}$ . In the cosmological case  $\Delta t \simeq H^{-1}$ . In the NS case one may naively think that this is replaced by the characteristic time scale of the merger, namely by a few milliseconds. However, the effective time duration is shorter. The reason is that, once a GW produced inside the HoCS leaves the HoCS, it no longer contributes to the growth of  $\rho_{\text{GW}}$  inside the HoCS. The effective time scale to determine the GW energy density inside the HoCS is therefore the light-crossing time of the HoCS

$$\Delta t \simeq L \simeq 1.7 \times 10^{-2} \text{ ms}, \quad (3.6)$$

where we have used (1.1).

$R$  is a characteristic length scale in the fluid flow which must be present in (3.1) on dimensional grounds once the rest of the dimensionful factors have been identified. The presence of this scale is also confirmed by explicit simulations that show that this scale coincides with the mean separation between the bubbles whose collisions produce the fluid flow in the first place.

Finally,  $\bar{\Omega}_{\text{GW}}$  is a dimensionless factor quantifying the efficiency with which shear stress in the fluid is converted to GWs. Although its precise value depends on the details of the flow, simulations show that its ballpark value,  $\bar{\Omega}_{\text{GW}} \sim 10^{-2}$ , is rather insensitive to these details.

The GW energy density is related to the characteristic strain  $h_c$  through (see e.g. [20])

$$\rho_{\text{GW}} = \frac{2\pi^2}{8\pi G} \frac{h_c^2}{\lambda^2}. \quad (3.7)$$

Equating (3.1) and (3.7) we find

$$h_c^2 \simeq \frac{10^6}{2\pi^2} v_f^4 \left( \frac{\mathcal{E} + \mathcal{P}}{M_p^4} \right) \left( (\mathcal{E} + \mathcal{P}) \times 1\text{ms} \times 1\text{m}^3 \right) \bar{\Omega}_{\text{GW}} \left( \frac{\Delta t}{1 \text{ ms}} \right) \left( \frac{\lambda}{100 \text{ m}} \right)^3, \quad (3.8)$$

where we have used (2.1). The second and third factors are

$$\frac{\mathcal{E} + \mathcal{P}}{M_p^4} \simeq 4.8 \times 10^{-76}, \quad (\mathcal{E} + \mathcal{P}) \times 1\text{ms} \times 1\text{m}^3 \simeq 3 \times 10^{66}. \quad (3.9)$$

Putting it all together we get

$$h_c \simeq 8.5 \times 10^{-4} v_f^2 \left( \frac{\Delta t}{1\text{ms}} \right)^{1/2} \left( \frac{\lambda}{100\text{m}} \right)^{3/2}. \quad (3.10)$$

The amplitude of the GW decreases as the inverse distance  $d$  to the source, so the observed characteristic strain would be

$$h_c^{\text{obs}} = h_c \frac{L}{d} \simeq 1.4 \times 10^{-24} v_f^2 \left( \frac{100\text{Mpc}}{d} \right) \left( \frac{\Delta t}{1\text{ms}} \right)^{1/2} \left( \frac{\lambda}{100\text{m}} \right)^{3/2}. \quad (3.11)$$

Using the values (2.23) and (3.6) we finally arrive at

$$h_c^{\text{obs}} \simeq 2.1 \times 10^{-24} v_f^2 \left( \frac{100\text{Mpc}}{d} \right). \quad (3.12)$$

The fluid velocity depends on details of the phase transition such as the strength of the transition, the bubble wall velocity, etc., but a representative range is [21]

$$0.01 \lesssim v_f \lesssim 0.3, \quad (3.13)$$

with higher values favoured for strong phase transitions, as might be expected for QCD. It is conceivable that future superconducting radio-frequency GW detectors may reach a sensitivity of order  $h_c \simeq 10^{-24}$  [22, 23]. If we require that the observed characteristic strain be at least as large as this value, then the velocity range (3.13) translates into a range of maximum distances from which the signal could be observed given by

$$20\text{kpc} \lesssim d \lesssim 20\text{Mpc}. \quad (3.14)$$

For comparison, for the first detection GW170817 [24] the distance was  $d \simeq 40\text{Mpc}$ .

## 4 Discussion

Numerical simulations of NS mergers based on a QCD EoS with a FOPT show that the phase transition is accessed during the merger dynamics. We have argued that, because the characteristic time scale of the merger evolution is so much longer than the nuclear time scale, from the QCD viewpoint the evolution is adiabatic to an extremely good approximation. This results in the formation of metastable regions of superheated and/or supercompressed matter in which the phase transition takes place via the formation and subsequent expansion and collision of bubbles.

This physics is analogous to that of a cosmological phase transition, except for the fact that in the cosmological case the metastable region is supercooled. Based on this analogy we have provided a rough estimate of the features of the resulting GW spectrum. We have

found that the duration of the signal is of order of milliseconds and the peak frequency is in the MHz range. Based on the analogy with the cosmological case, we expect the precise GW power spectrum to take the form a broken power law centered around this frequency.

The characteristic strain that would be observed coming from a single superheated and/or supercompressed spot is given by (3.12). Simulations show that several spots are typically formed, and that they can transition back to the original phase. This transition would proceed via the nucleation and collision of supercooled bubbles, leading to additional emission of GWs in a similar frequency range. We expect these effects to enhance the signal that we have estimated.

Our results are interesting for several reasons. First, this is the only known *astrophysical* source of GWs in the MHz range. Second, as indicated by eqn. (3.14), it is conceivable that signals coming from NS mergers as far as tens of Mpc might be detectable by future superconducting radio-frequency GW detectors [22, 23]. Given all the uncertainties in our rough estimate, we regard this as an exciting outcome. Third, the detection of the MHz signal would be aided (i) by the fact that it would happen at the same time as the usual kHz signal associated to the merger, and (ii) by the fact that both would be preceded by the long inspiral signal, which for GW170817 lasted for about 100 s. Fourth, the signal is stochastic in nature, since it originates from the superposition of the dynamics of many sound waves, but it will come from a very specific direction in the sky determined by the location of the NS binary. All these considerations suggest that, with the targeted sensitivity of future detectors in the MHz range, GWs may provide us with a direct signal of a FOPT in QCD.

## Acknowledgements

We are grateful to Jordi Miralda for collaboration at the initial stages of this paper, and to Krishna Rajagopal for comments on the draft. We thank Yago Bea, Roberto Emparan, Alexander Haber, Luciano Rezzolla, Andreas Schmitt, Alexandre Serantes, and specially Andreas Ringwald and Carlos Tamarit, for useful discussions. We are extremely grateful to Diego Blas for extensive explanations. We are supported by the “Unit of Excellence MdM 2020-2023” award to the Institute of Cosmos Sciences (CEX2019-000918-M) and by grants SGR-2017-754, PID2019-105614GB-C21 and PID2019-105614GB-C22. MSG is also supported by the European Research Council (ERC) under the European Union’s Horizon 2020 research and innovation program (grant agreement No758759).

## References

- [1] L. Baiotti and L. Rezzolla, *Binary neutron star mergers: a review of Einstein’s richest laboratory*, *Rept. Prog. Phys.* **80** (2017) 096901 [[1607.03540](#)].
- [2] P. de Forcrand, *Simulating QCD at finite density*, *PoS LAT2009* (2009) 010 [[1005.0539](#)].
- [3] M. Stephanov, *The phase diagram of QCD and the critical point*, *Acta Phys. Polon. B* **35** (2004) 2939.

- [4] M.G. Alford, A. Schmitt, K. Rajagopal and T. Schäfer, *Color superconductivity in dense quark matter*, *Rev. Mod. Phys.* **80** (2008) 1455 [[0709.4635](#)].
- [5] K. Fukushima and T. Hatsuda, *The phase diagram of dense QCD*, *Rept. Prog. Phys.* **74** (2011) 014001 [[1005.4814](#)].
- [6] J.N. Guenther, *An overview of the QCD phase diagram at finite  $T$  and  $\mu$* , in *38th International Symposium on Lattice Field Theory*, 1, 2022 [[2201.02072](#)].
- [7] E.R. Most, L.J. Papenfort, V. Dexheimer, M. Hanauske, S. Schramm, H. Stöcker and L. Rezzolla, *Signatures of quark-hadron phase transitions in general-relativistic neutron-star mergers*, *Phys. Rev. Lett.* **122** (2019) 061101 [[1807.03684](#)].
- [8] E.R. Most, L. Jens Papenfort, V. Dexheimer, M. Hanauske, H. Stoecker and L. Rezzolla, *On the deconfinement phase transition in neutron-star mergers*, *Eur. Phys. J. A* **56** (2020) 59 [[1910.13893](#)].
- [9] C. Ecker, M. Järvinen, G. Nijs and W. van der Schee, *Gravitational waves from holographic neutron star mergers*, *Phys. Rev. D* **101** (2020) 103006 [[1908.03213](#)].
- [10] A. Prakash, D. Radice, D. Logoteta, A. Perego, V. Nedora, I. Bombaci, R. Kashyap, S. Bernuzzi and A. Endrizzi, *Signatures of deconfined quark phases in binary neutron star mergers*, *Phys. Rev. D* **104** (2021) 083029 [[2106.07885](#)].
- [11] L.R. Weih, M. Hanauske and L. Rezzolla, *Postmerger Gravitational-Wave Signatures of Phase Transitions in Binary Mergers*, *Phys. Rev. Lett.* **124** (2020) 171103 [[1912.09340](#)].
- [12] S. Tootle, C. Ecker, K. Topolski, T. Demircik, M. Järvinen and L. Rezzolla, *Quark formation and phenomenology in binary neutron-star mergers using V-QCD*, [2205.05691](#).
- [13] M.B. Hindmarsh, M. Lüben, J. Lumma and M. Pauly, *Phase transitions in the early universe*, *SciPost Phys. Lect. Notes* **24** (2021) 1 [[2008.09136](#)].
- [14] Y. Bea, J. Casalderrey-Solana, T. Giannakopoulos, A. Jansen, D. Mateos, M. Sanchez-Garitaonandia, A. Serantes and M. Zilhão, *Superheated and/or Supercompressed Relativistic Bubbles*, in preparation.
- [15] M. Hindmarsh, S.J. Huber, K. Rummukainen and D.J. Weir, *Gravitational waves from the sound of a first order phase transition*, *Phys. Rev. Lett.* **112** (2014) 041301 [[1304.2433](#)].
- [16] M. Hindmarsh, S.J. Huber, K. Rummukainen and D.J. Weir, *Numerical simulations of acoustically generated gravitational waves at a first order phase transition*, *Phys. Rev. D* **92** (2015) 123009 [[1504.03291](#)].
- [17] E. Annala, T. Gorda, A. Kurkela, J. Nättilä and A. Vuorinen, *Evidence for quark-matter cores in massive neutron stars*, *Nature Phys.* **16** (2020) 907 [[1903.09121](#)].
- [18] A.H. Guth and E.J. Weinberg, *Cosmological Consequences of a First Order Phase Transition in the  $SU(5)$  Grand Unified Model*, *Phys. Rev. D* **23** (1981) 876.
- [19] K. Enqvist, J. Ignatius, K. Kajantie and K. Rummukainen, *Nucleation and bubble growth in a first order cosmological electroweak phase transition*, *Phys. Rev. D* **45** (1992) 3415.
- [20] C.J. Moore, R.H. Cole and C.P.L. Berry, *Gravitational-wave sensitivity curves*, *Class. Quant. Grav.* **32** (2015) 015014 [[1408.0740](#)].
- [21] D. Cutting, M. Hindmarsh and D.J. Weir, *Vorticity, kinetic energy, and suppressed gravitational wave production in strong first order phase transitions*, *Phys. Rev. Lett.* **125** (2020) 021302 [[1906.00480](#)].

- [22] A. Ringwald, private communication.
- [23] R.T. D’Agnolo, *Microwave cavities*, talk at the “Ultra-High-Frequency GWs: A Theory and Technology Roadmap” workshop, CERN, Oct 12-15, 2021.
- [24] LIGO SCIENTIFIC, VIRGO collaboration, *GW170817: Observation of Gravitational Waves from a Binary Neutron Star Inspiral*, *Phys. Rev. Lett.* **119** (2017) 161101 [[1710.05832](#)].